SPACE SCIENCES

The initial solar system abundance of ^{60}Fe and early core formation of the first asteroids

Linru Fang[1]*, Frédéric Moynier[1], Marc Chaussidon[1], Angela Limare[1], Georgy V. Makhatadze[1], Johan Villeneuve[2]

High-precision Ni isotope analyses of the differentiated andesitic meteorite Erg Chech 002 (EC 002), the oldest known crustal fragment of a planetesimal, show that short-lived ^{60}Fe was present in the early solar system with an initial ^{60}Fe/^{56}Fe ratio of $(7.71 \pm 0.47) \times 10^{-9}$, which is five times more precise than previous estimates and is proposed to be the reference value for further studies. Using this ratio, the Ni isotopic composition of EC 002 implies that metal segregation in the source of the EC 002 parental melts took place $0.82^{+0.61}_{-0.60}$ million years (Myr) after solar system formation, and similar very early metal-silicate differentiation ages are obtained for 4-Vesta ($0.95^{+0.95}_{-0.76}$ Myr) and the angrite parent body ($2.27^{+1.98}_{-1.29}$ Myr). Such an early age dictates a specific accretion and differentiation history for the EC 002 parent body, with metal segregation occurring at relatively low temperatures (1000° to 1200°C), followed by a high-temperature silicate melting event.

INTRODUCTION

Short-lived radioactive (SLR) systems (e.g., ^{26}Al-^{26}Mg, ^{53}Mn-^{53}Cr, ^{60}Fe-^{60}Ni, ^{182}Hf-^{182}W, and ^{146}Sm-^{142}Nd) are key to establish a relative chronology of events that took place during the early solar system (ESS), such as condensation processes, chondrule formation, core-mantle differentiation, and crystallization of magma oceans in planetary bodies [e.g., (*1*)]. ^{26}Al is an SLR isotope ($T_{1/2} = 0.705 \pm 0.024$ Myr) (*2*) of a major element making terrestrial planets. As such, even before its discovery in the Ca-Al–rich inclusions (CAIs) of the CV3 chondrite Allende (*3*), its decay was proposed to be a major heat source responsible for the rapid differentiation of planetary bodies accreted during the first few million years (Myr) of the accretion disk (*4*). This could also be the case for ^{60}Fe ($T_{1/2} = 2.62 \pm 0.04$ Myr) (*5*) discovered in the eucritic differentiated meteorite Chervony Kut (*6*), with the specificity that ^{60}Fe decay could produce heat in the metallic core as well as in the mantle of planetary bodies. However, the role that ^{60}Fe could have played depends on its abundance [e.g., (*7*)] in the ESS. Proposed levels span three orders of magnitude, with ^{60}Fe/^{56}Fe ranging from 10^{-9} to 10^{-6} (*8*–*13*). While this range of variations could, in theory, reflect a strong heterogeneity in the distribution of ^{60}Fe in the ESS, it seems more likely that the high abundances of ^{60}Fe (^{60}Fe/^{56}Fe ≈ 2 to 9×10^{-7}) inferred from isochrons obtained by various ion microprobe studies (*12*–*14*) suffer from some analytical biases, even if these biases have not yet been all firmly established. Possible sources of bias could be very low count rates (dynamic background corrections and isotopic ratio calculation), potential interferences, or secondary micrometer scale redistribution of radiogenic Ni by diffusion (*14*–*18*). Studies using bulk or mineral separates limit the possible bias introduced on the ion microprobe ^{60}Fe isochrons by micrometer-scale redistribution of Fe and Ni isotopes. Taking advantage of the high-precision Ni isotope data from multicollector inductively coupled plasma mass spectrometer (MC-ICP-MS), bulk studies apart from (*11*) yield low ^{60}Fe abundances, consistent with the Chervony Kut ^{60}Fe/^{56}Fe ratio of $\sim 3.9 \times 10^{-9}$ (*6*), implying an initial ^{60}Fe/^{56}Fe ratio of the solar system around 10^{-8}. This is the case for sulfides from IVA iron meteorites (*9*) and for basalts from differentiated asteroids (such as angrites, eucrites, and diogenites) as well as of chondrules from unequilibrated ordinary (UOC) and CB chondrites that point to a homogeneous distribution of ^{60}Fe in the solar system with an initial ^{60}Fe/^{56}Fe ratio of $(10.1 \pm 2.7) \times 10^{-9}$ (*10*, *19*).

Improving the estimates of the ^{60}Fe abundance in the ESS is necessary to further assess its homogeneity and to develop the use of the ^{60}Fe-^{60}Ni system as a chronometer for dating early accretion and differentiation events. Progress can be made by studying samples of the crust from a parent body (thus with large Fe/Ni fractionation due to metal-silicate and possible silicate-silicate differentiation) that differentiated very early [thus minimizing error propagation when back-calculating the solar system initial (SSI) ^{60}Fe/^{56}Fe]. In this respect, the Erg Chech 002 (EC 002) achondrite presently is the best-suited sample as it is the oldest volcanic and andesitic achondrite discovered to date, with a crystallization age of 1.80 ± 0.01 Myr after CAIs as indicated by ^{26}Al chronology on mineral separates (*20*). The closure temperature of Al-Mg [e.g., in plagioclase: 450° to 520°C; (*21*)] and Fe-Ni [400–500°C; (*22*)] systems is similar; meanwhile, the cooling rate of EC 002 below 900°C is very rapid [>0.1 to 1°C/day; (*23*)]; thus, the closing time of these two chronometers should be nearly the same. EC 002 is therefore expected to exhibit prominent ^{60}Ni excesses and offer strong constraints on the initial ^{60}Fe/^{56}Fe ratio, for both EC 002 itself and the ESS.

EC 002 is an ungrouped achondrite with a large recovered mass (~32 kg). It has an unbrecciated igneous texture and is composed of pyroxene and olivine megacrysts and medium-grained groundmass [1 to 1.5 mm, consisting of albitic feldspar (45 vol. %), pyroxene (38 vol. %) and a few interstitial silica minerals, spinel, ilmenite, troilite, phosphates, and Fe-Ni metal] (*23*). EC 002 has a flat CI-normalized rare earth element distribution pattern (*23*) but fractionated and relatively low highly siderophile element abundances compared to CI chondrites (*24*). The neodymium [μ^{148}Nd = 12 ± 3.6 parts per million (ppm)], oxygen ($\Delta^{17}O = -0.136 \pm 0.018$‰), and chromium ($\varepsilon^{54}Cr = -0.726 \pm 0.112$‰) isotopic compositions of EC 002 indicate that the parent body of EC 002 formed within the noncarbonaceous reservoir (*20*, *25*, *26*). With the old crystallization age, large recovered mass, abundant coarse mineral grains, and trace

[1]Université Paris Cité, Institut de Physique du Globe de Paris, CNRS, Paris 75005, France. [2]Université de Lorraine, CNRS, CRPG, UMR7358, F-54000 Nancy, France.
*Corresponding author. Email: lfang@ipgp.fr

element-enriched components, EC 002 holds great potential as an anchor for various short-lived radioactive systems (e.g., ^{26}Al-^{26}Mg, ^{146}Sm-^{142}Nd, and probably ^{60}Fe-^{60}Ni) and therefore to define the initial abundance of short-lived parent nuclides (*20*) and constrain their distribution throughout the solar system.

Here, we used several separating techniques to yield 14 fractions of EC 002 with a broad range of ^{56}Fe/^{58}Ni molar ratios (6.2×10^3 to 6.5×10^5, table S1), which is much wider than previous Fe-Ni internal isochrons (*10*, *19*, *27*). With the help of high-sensitivity MC-ICP-MS analyses [signal on ^{58}Ni is ~160 V/ppm, two to three times more than previously reported (*10*)], we obtained high-precision Ni isotope data on these bulk fractions and mineral separates. These results yield a well-defined ^{60}Fe-^{60}Ni isochron for EC 002 and allow to improve the precision of the initial ^{60}Fe abundance in the solar system by a factor of 5, and to show how high-precision ^{60}Fe/^{56}Fe ratios in planetesimals can help constrain their accretion and differentiation history.

RESULTS

To correct for any mass-dependent isotopic fractionation, the measured ^{60}Ni/^{58}Ni ratios are normalized to a ^{61}Ni/^{58}Ni ratio of 0.016744 (*28*) using an exponential law (*29*), and ^{60}Ni excesses are expressed as the per-10,000 deviations from the pure Ni standard NIST SRM 986: $\varepsilon^{60}Ni_{61/58} = [(^{60}Ni/^{58}Ni)_{sample}/(^{60}Ni/^{58}Ni)_{SRM986} - 1] \times 10{,}000$. The ^{60}Ni excess of geo-standards AGV-2 and BHVO-2 was measured at -0.05 ± 0.21 ($N = 13$) and 0.21 ± 0.17 ($N = 13$), respectively (table S1), consistent with previous studies of terrestrial rocks (*10*). Unless otherwise specified, errors in this text are reported as twice the standard error (2σ).

The $\varepsilon^{60}Ni_{61/58}$ values and ^{56}Fe/^{58}Ni molar ratios for both the bulk and mineral separates of EC 002 define a well-correlated linear relationship (Fig. 1) with a mean square of the weighted deviation (MSWD) of 1.5 (the MSWD 95% confidence interval is between 0.4 and 1.9), determined by the least square regression calculation (*30*) using CEREsFit (*31*). The slope and intercept of this regression line are 0.0001304 ± 0.0000029 and 0.20 ± 0.14, respectively. The initial ^{60}Fe and ^{60}Ni abundances of EC 002 were estimated based on the slope and intercept of the ^{60}Fe isochron: $\varepsilon^{60}Ni_{present} = \varepsilon^{60}Ni_{0\text{-}EC\ 002} + (^{58}Ni/^{60}Ni)_{standard} \times 10^4 \times (^{60}Fe/^{56}Fe)_{0\text{-}EC\ 002} \times (^{56}Fe/^{58}Ni)_{present}$, where $(^{58}Ni/^{60}Ni)_{standard}$ is equal to 2.5961, corresponding to the reference value of standard SRM 986 (*28*). This gives a value of $(^{60}Fe/^{56}Fe)_{0\text{-}EC\ 002}$ of $(5.02 \pm 0.11) \times 10^{-9}$ (2σ), which is the most precise ^{60}Fe/^{56}Fe ratio constrained by an internal ^{60}Fe-^{60}Ni isochron to date (*10*, *19*, *27*). The $\varepsilon^{60}Ni_{0\text{-}EC\ 002}$ is $+0.20 \pm 0.14$ (2σ), slightly higher than that of differentiated meteorites such as angrites, eucrite, and diogenite (−0.10 to +0.08) (*10*, *27*). The details of the approach used to ensure the best reliability and accuracy to determine $(^{60}Fe/^{56}Fe)_{0\text{-}EC\ 002}$ and $\varepsilon^{60}Ni_{0\text{-}EC\ 002}$ are given in the Supplementary Materials.

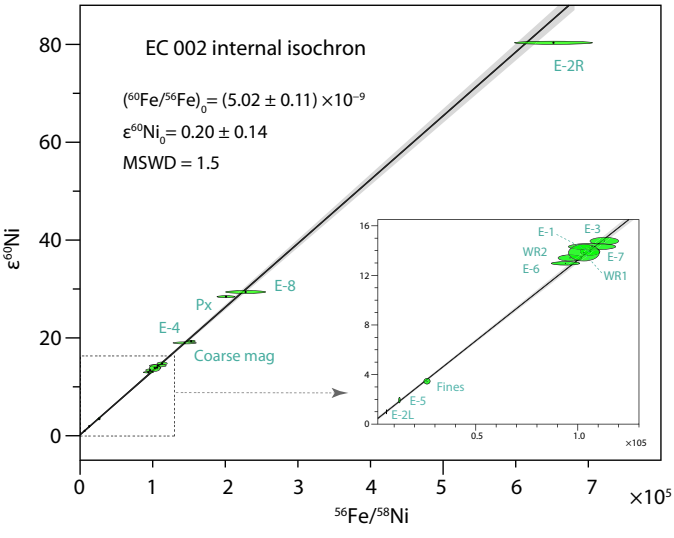

Fig. 1. Internal ^{60}Fe-^{60}Ni isochron of EC 002. The ε^{60}Ni values were normalized to ^{61}Ni/^{58}Ni. The slope and intercept of this isochron are 0.0001304 ± 0.0000029 and + 0.20 ± 0.14, respectively, which returns a ^{60}Fe/^{56}Fe ratio of (5.02 ± 0.11) × 10^{-9} and a ε^{60}Ni value of +0.20 ± 0.14 for EC 002 at its crystallization. The regression is based on a least square algorithm (*30*) using the software tool CEREsFIT.xlsm (*31*).

DISCUSSION

Solar system initial ^{60}Fe abundance

The antiquity of EC 002 has been established through various radioactive dating systems, including both long-lived and short-lived dating systematics such as ^{26}Al-^{26}Mg, ^{53}Mn-^{53}Cr, ^{40}K-^{40}Ca, ^{147}Sm-^{143}Nd, and U-corrected Pb-Pb (see table S2). However, the discrepancies in reported absolute crystallization ages of 4565.87 ± 0.30 Ma (*32*), 4566.19 ± 0.20 Ma (*33*), or 4565.56 ± 0.12 Ma (*34*) by U-corrected Pb-Pb systematics pose challenges for properly anchoring EC 002. To address this issue, we combined the U isotopic compositions [^{238}U/^{235}U = 137.821 ± 0.022; an average value of 137.813 ± 0.01 (*33*) and 137.8288 ± 0.0054 (*34*) determined by whole rock fractions] and Pb isotopic data from (*33*) and (*34*), and obtained an inversed U-corrected Pb-Pb age of 4565.68 Ma (fig. S5), i.e., 1.62 Myr after CAIs (*35*). When both the errors from the Pb-Pb isochron and from the variation of their reported ^{238}U/^{235}U ratios were propagated, the Pb-Pb age error is estimated to be 0.21 Ma (2σ). Lead isotopic data from (*32*) were not incorporated because they did not provide the error correlation coefficients between the ^{204}Pb/^{206}Pb and ^{207}Pb/^{206}Pb ratios.

Using this Pb-Pb age (4565.68 ± 0.21 Ma) and the $(^{60}Fe/^{56}Fe)_{0\text{-}EC\ 002}$ of $(5.02 \pm 0.11) \times 10^{-9}$, the SSI ^{60}Fe/^{56}Fe ratio was back-calculated to be $(7.71 \pm 0.47) \times 10^{-9}$ (Fig. 2) at the Pb-Pb age of CAIs of 4567.3 Ma (*35*). This value is consistent within error with the average $(^{60}Fe/^{56}Fe)_{SSI}$ ratio of $(10.1 \pm 2.7) \times 10^{-9}$ determined based on bulk analyses of UOC and CB chondrules, angrites and HED meteorites anchored to the same CAI age (*10*, *19*). Note that the $(^{60}Fe/^{56}Fe)_{SSI}$ ratio would obviously be higher (~10 to 11 × 10^{-9}) assuming an older age for the solar system (4568.4 or 4568.7 Ma), if considering that the Pb-Pb age of CAIs is different as proposed by Piralla *et al.* (*36*) and Desch *et al.* (*37*), while resolving the issue of the age of the solar system is beyond the scope of the present work.

A $(^{60}Fe/^{56}Fe)_{SSI}$ ratio of $(7.71 \pm 0.47) \times 10^{-9}$ is more precise than estimates, which can be made from previous data for the angrite D'Orbigny and the whole-rock HED meteorites (most likely from asteroid 4-Vesta) that indicate $(^{60}Fe/^{56}Fe)_{SSI}$ ratios of $(14.7 \pm 4.6) \times 10^{-9}$ and $(10.2 \pm 3.2) \times 10^{-9}$, respectively (*10*). The crystallization ages of D'Orbigny (5.5 ± 1.0 Myr) and the mantle differentiation time of 4-Vesta (4.1 ± 1.1 Myr) relative to CAIs used in (*10*) for back-calculating the $(^{60}Fe/^{56}Fe)_{SSI}$ ratios were defined from the ^{53}Mn-^{53}Cr systematics. However, the U-corrected Pb-Pb chronometer showed a

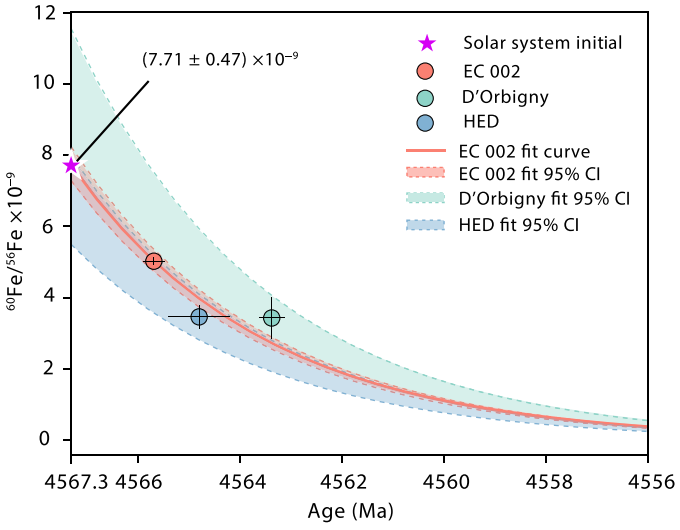

Fig. 2. The solar system initial $^{60}Fe/^{56}Fe$ defined by initial $^{60}Fe/^{56}Fe$ values and corresponding crystallization ages of EC 002 and other differentiated meteorites. The $^{60}Fe/^{56}Fe$ evolution curve and ranges were constrained by the ages and $^{60}Fe/^{56}Fe$ values of EC 002 (red field), D'Orbigny (green field), and HED meteorites (blue field). The crystallization age of angrite D'Orbigny is 4563.37 ± 0.25 Ma dated by the Pb-Pb chronometer (*38*) and the mantle differentiation time of the parent body of HED meteorites was calculated using their initial $^{53}Mn/^{55}Mn$ value [(4.21 ± 0.46) × 10^{-6}, (*40*)] relative to that of D'Orbigny [(3.24 ± 0.04) × 10^{-6}, (*39*)] and the Pb-Pb absolute age of D'Orbigny. The initial $^{60}Fe/^{56}Fe$ values of D'Orbigny and HED meteorites are from (*10*). All dashed lines show the boundaries of 95% confidence interval (95% CI).

more precise absolute crystallization age of D'Orbigny of 4563.37 ± 0.25 Ma (*38*), which is 3.93 ± 0.25 Myr after CAIs formations (*35*). Using this crystallization age and the initial $^{53}Mn/^{55}Mn$ ratios of D'Orbigny (*39*) and whole-rock HED meteorites (*40*), the mantle differentiation time of 4-Vesta was constrained to be 2.51 ± 0.60 Myr after CAIs. According to these more precise ages, the $(^{60}Fe/^{56}Fe)_{SSI}$ ratios anchored to D'Orbigny and whole-rock HED meteorites were recalculated to be (9.70 ± 1.76) × 10^{-9} and (6.70 ± 1.23) × 10^{-9}. These $(^{60}Fe/^{56}Fe)_{SSI}$ ratios are consistent within errors but still less precise than the one estimated using EC 002 (Fig. 2). The five times higher precision obtained for the present SSI is due to the more precise $^{60}Fe/^{56}Fe$ ratio of EC 002 as well as its older, and more precise Pb-Pb crystallization age.

The $(^{60}Fe/^{56}Fe)_{SSI}$ ratios deduced from chondrules using in situ measurements [ranging from 2 × 10^{-7} to 1 × 10^{-6} (*12*, *14*, *15*, *41*)] are two orders of magnitude higher than the ratio calculated from EC 002 [(7.71 ± 0.47) × 10^{-9}]. The potential bias during data reduction of in situ measurements was reported to be less than 0.5‰ when taking the sum of the total counts to calculate the ratios, which is negligible compared to typical errors of ~20‰ (*41*). Therefore, the more likely factor for this discrepancy is micro-scale Fe-Ni mobilization during parent body processes and/or during terrestrial weathering, which could result in both high and low estimates of the initial $^{60}Fe/^{56}Fe$ ratios (*16*). Considering potential Fe-Ni redistribution in chondrules, a lower limit of 5 × 10^{-8} for the initial $^{60}Fe/^{56}Fe$ ratio of the region where UOC chondrules formed was constrained using the 20‰ excesses in ^{60}Ni measured in chondrules, assuming a maximum $^{56}Fe/^{62}Ni$ ratio of 3 × 10^{6} for silicates in chondrules (*42*). The ^{60}Ni excesses in the chondrules from the least thermally metamorphosed ordinary chondrite (Semarkona LL3.00) were mostly unresolved within error, which was explained by the postcrystallization redistribution of Ni and/or Fe (*42*). However, such secondary perturbations were not observed by a subsequent high-precision (<5‰) in situ study using resonance ionization mass spectrometry on Semarkona chondrule DAP1, thus suggesting a low SSI ^{60}Fe abundance (*17*). Further in situ Fe-Ni isotope analyses on type 3 chondrites troilites, for which no Fe-Ni remobilization was detected, inferred an initial $^{60}Fe/^{56}Fe$ ratio of (1.05 ± 1.48) × 10^{-8} (*18*). These low $^{60}Fe/^{56}Fe$ ratios in chondrules are in line with the present $(^{60}Fe/^{56}Fe)_{SSI}$ inferred from EC 002.

The potential disturbance of the Fe-Ni systematics is also a main challenge during bulk analyses on early formed objects such as CAIs, chondrules, and differentiated meteorites (*8*, *10*, *16*, *43*, *44*). Both terrestrial contamination and parent body aqueous alteration involve fluid re-mobilization of Ni and/or Fe, which could make the initial ^{60}Fe-^{60}Ni regression line flatter, resulting in lower apparent initial $^{60}Fe/^{56}Fe$ ratio (*16*). Commonly, ethanol and mild HCl leaching are used to remove the surface Fe and Ni contaminations in meteorites [e.g., (*10*)]. However, this leaching process could over-remove Ni for some eucrites (*44*). Here, we used three different mild ways (only MQ water, acetone + MQ water, and weak acid leaching) to wash mineral and bulk fractions of EC 002 before wet chemistry (Supplementary Materials). All the fractions aligned well on the regression line of $\varepsilon^{60}Ni_{61/58}$ values and $^{56}Fe/^{58}Ni$ ratios (Fig. 1), suggesting that our protocol removed contaminations efficiently without reaching the original Ni and Fe of EC 002. On the other hand, lattice diffusion of Ni may have occurred on thermally metamorphosed achondrites such as brecciated eucrites like Juvinas (*44*). In such a case, the pyroxene annealing might release Ni from pyroxene into chromite, leading to the high and low ^{60}Ni excesses relative to the best-fit line for chromite and pyroxene fractions observed in Juvinas (*44*). However, the Ni concentrations of ilmenite and Cr-spinel of EC 002 are very low, at the same magnitude as that in pyroxene (*26*). Besides, the Ni concentrations of pyroxene-enriched fractions (0.90 ppm, table S1) and olivine megacryst [1.31 ppm, (*23*)] of EC 002 are quite consistent, suggesting that no Ni was diffused from pyroxene to chromite. Despite the fact that lattice diffusion in sulfides could result in a poor correlation between the Ni isotopic composition and the Fe/Ni ratio (*16*), the low Ni concentration in sulfides and metals of EC 002 (*24*) indicates a negligible perturbation of Ni in these phases. Therefore, the unbrecciated nature of EC002 and the quality of the ^{60}Fe isochron imply a lack of substantial ^{60}Ni redistribution by metamorphism after its crystallization, suggesting that $(^{60}Fe/^{56}Fe)_{SSI}$ deduced from EC 002 is robust.

Currently, despite the limited number of data, no definitive claim can be made that ^{60}Fe was heterogeneously distributed in the ESS. As shown in fig. S6, a $(^{60}Fe/^{56}Fe)_{SSI}$ ratio of (7.71 ± 0.47) × 10^{-9} would be in line not only with data on angrites and HED meteorites (see discussion above) but also with data on chondrules from unequilibrated ordinary chondrites and CB carbonaceous chondrites. This does not point to a difference in the initial $^{60}Fe/^{56}Fe$ ratio between the noncarbonaceous reservoir [inner solar system as represented by EC 002 (*20*, *33*, *34*), angrites, HED meteorites, and UOC] and the carbonaceous reservoir (outer solar system as represented by the CB chondrules). In addition, the suggestion from a bulk Ni isotope study of IVB and IID carbonaceous iron meteorites (*11*) that the initial $^{60}Fe/^{56}Fe$ of the outer solar system could be as high as (6.4 ± 2.0) × 10^{-7} is lacking strong evidence because the two-point

model age used in (*11*) is highly dependent on the assumption that IVB and IID irons derived from a CI chondritic reservoir, while the variations of their Ni isotope anomalies (*45*, *46*) suggested that it might not be the case (see the Supplementary Materials).

Last, it is important to note that the $(^{60}Fe/^{56}Fe)_{SSI}$ ratio of $(7.71 \pm 0.47) \times 10^{-9}$ is notably lower than that predicted if ^{60}Fe in the ESS was injected by a type II supernova (10^{-7} to 10^{-5}) (*47*), which is confirmed by the simulations of 15 to 25 $M_{\odot}$ stars (*48*). Besides, note that the H-ingestion supernova models show that ^{26}Al could be injected with negligible ^{60}Fe (*49*). Overall, no compelling need exists for a ^{60}Fe late injection from a supernova, and the low SSI ^{60}Fe abundance was likely inherited from the interstellar medium (ISM). In addition, if the present $(^{60}Fe/^{56}Fe)_{ISM}$ ratio of $(2.8 \pm 1.4) \times 10^{-7}$ (*10*) was the same 4.6 billion years ago, which cannot be easily demonstrated (*50*), then isolating the parent molecular cloud a few Myr from injection of stellar products would reduce the $(^{60}Fe/^{56}Fe)_{SSI}$ ratio relative to the $(^{60}Fe/^{56}Fe)_{ISM}$ (*10*).

Time of metal segregation of the first asteroids

The $(^{60}Fe/^{56}Fe)_{SSI}$ ratio of $(7.71 \pm 0.47) \times 10^{-9}$, a CI chondrite Fe/Ni ratio [17.2 (*51*)], and the present-day $\varepsilon^{60}Ni = 0$ of Earth imply an SSI $\varepsilon^{60}Ni_{SSI}$ of −0.005 and a nearly flat growth curve of $\varepsilon^{60}Ni$ in the solar system (Fig. 3), assuming a homogeneous distribution of ^{60}Fe and ^{60}Ni in the ESS. Using the Fe/Ni ratios of 2804 and 2244 for the bulk silicate 4-Vesta and angrite parent body (APB), as estimated from the chemical composition of the corresponding meteorites (*52*) and through ^{60}Fe-^{60}Ni external isochron/errorchron (*10*), the $\varepsilon^{60}Ni$ values at the time of mantle differentiation ($\varepsilon^{60}Ni_{mantle}$) for 4-Vesta and APB are estimated to be 0.259 ± 0.136 and 0.164 ± 0.141, respectively (fig. S9; see the error propagation in the Supplementary Materials). For EC 002, the $\varepsilon^{60}Ni$ value at its crystallization (i.e., the intercept of EC 002 internal isochron, $\varepsilon^{60}Ni_{0\text{-EC 002}} = 0.20 \pm 0.14$, Fig. 1) represents the $\varepsilon^{60}Ni$ value of its parental melts, whose source has not experienced any previous silicate differentiation event (*23*), but just metal segregation. In the following, the terms silicate differentiation and metal segregation refer to the source region of the EC 002 parent melt, while the terms mantle differentiation and core segregation refer to bulk 4-Vesta and APB. It is notable that the $\varepsilon^{60}Ni_{0\text{-EC 002}}$ value and $\varepsilon^{60}Ni_{mantle}$ values for 4-Vesta and APB all plot above the solar system evolution curve (Fig. 3). This can indicate either that these different parent bodies formed from precursors with different nucleosynthetic excesses of ^{60}Ni, or that radiogenic ^{60}Ni excesses developed in these parent bodies due to the Fe/Ni fractionation following core segregation/metal segregation. The first possibility can be tested by looking at neutron-poor Ni isotopic anomalies, such as the $\varepsilon^{58}Ni_{62/61}$ ($\approx 3 \times \varepsilon^{62}Ni_{61/58}$) values. Nonradiogenic $\varepsilon^{60}Ni_{62/61}$ can be estimated using the trend existing between $\varepsilon^{58}Ni_{62/61}$ and $\varepsilon^{60}Ni_{62/61}$ (see fig. S7 and an explanation in the Supplementary Materials). This approach would give nonradiogenic $\varepsilon^{60}Ni_{62/61}$ values of −0.06 ± 0.03 and −0.06 ± 0.08 for angrites and HED meteorites according to their $\varepsilon^{62}Ni_{61/58}$ values (*10*), which cannot be resolved from each other, suggesting limited ^{60}Ni nucleosynthetic variations among the regions where these parent bodies formed. We thus explore in the second hypothesis whether the higher $\varepsilon^{60}Ni$ values at the time of mantle differentiation/silicate differentiation derived from the ^{60}Fe isochrons are the result of radiogenic ingrowth of ^{60}Ni after core formation/metal segregation.

The Fe/Ni ratio for the EC 002 forming region after metal segregation, and for the mantle of 4-Vesta and APB after core formation,

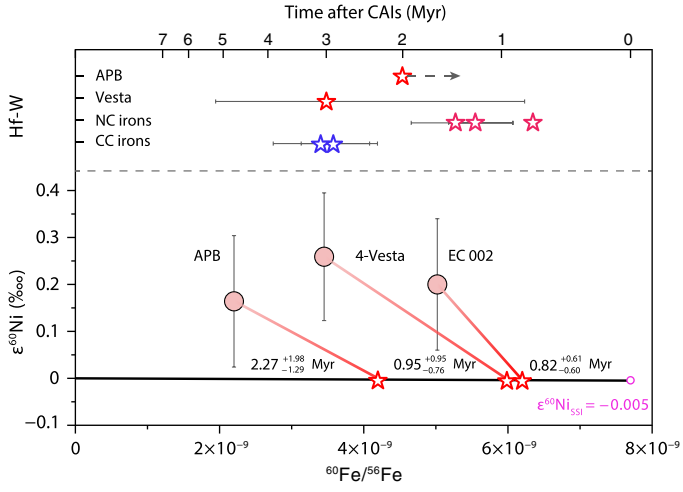

Fig. 3. Growth curves of $\varepsilon^{60}Ni$ for the solar system, the EC 002 parental melts forming-region, 4-Vesta, and the angrite parent body (APB). The solar system growth curve is anchored to $(^{60}Fe/^{56}Fe)_{SSI} = (7.71 \pm 0.47) \times 10^{-9}$ and $\varepsilon^{60}Ni_{SSI} = -0.005$ calculated assuming a CI chondrite Fe/Ni ratio of 17.2 for the solar system (*51*) and a present-day solar system $\varepsilon^{60}Ni = 0$. The growth curves of the EC 002, the APB, and 4-Vesta are calculated for a simple two-stage history: (i) a growth of $\varepsilon^{60}Ni$ in a reservoir with a chondritic Fe/Ni ratio (either the solar accretion disk or the undifferentiated body) and (ii) a growth of $\varepsilon^{60}Ni$ in the silicate portion (red lines) of the body remaining after metal segregation and fractionation of the Fe/Ni ratios to values of 4703, 2804, and 2244 for the EC 002, 4-Vesta, and APB (*52*), respectively. The growth curves of the silicate fractions of the bodies after metal segregation are anchored at the times of silicate differentiation for EC 002 forming region, and mantle differentiation for 4-Vesta and APB (red solid circles). The external ^{60}Fe isochrons reported in (*10*) with the bulk silicate Fe/Ni ratio from (*52*) give $\varepsilon^{60}Ni$ values at the time of mantle differentiation of 0.259 ± 0.136 and 0.164 ± 0.141 for 4-Vesta and APB (fig. S9). In this model, the intersection between the chondritic growth curve and the parent bodies growth curves determines the age of metal segregation (red stars, see the Supplementary Materials for error propagation). The core segregation ages derived from the Hf/W systematics for NC and CC iron meteorites (*55*), 4-Vesta (*53*), and APB (*54*) are plotted at the upper part of the diagram for comparison.

estimated to be at around 4703, 2804, and 2244, respectively (*52*), could reflect this radiogenic ingrowth. According to the intersection of the solar system $\varepsilon^{60}Ni$ growth curve and the second-stage $\varepsilon^{60}Ni$ growth curves for the EC 002 forming region, the time of metal segregation (t_{metal}) is estimated to be $0.82^{+0.61}_{-0.60}$ Myr after CAIs formation (Fig. 3). Following the same logic, the core formation ages (t_{core}) of 4-Vesta and APB are constrained to be $0.95^{+0.95}_{-0.76}$ and $2.27^{+1.98}_{-1.29}$ Myr after CAIs formation, respectively (Fig. 3) (see the error propagation in the Supplementary Materials). Other modeling for constraining the metal segregation time of planetesimals using ^{60}Fe-^{60}Ni isotope data have been conducted [e.g., (*10*)], but the one used in this study is more accurate (see the Supplementary Materials).

The only previous time constraints on core segregation were based on ^{182}Hf-^{182}W systematics of HED [3.3 ± 1.4 Myr after CAIs formation (*53*)] and of angrites [within 2 Myr after CAIs formation (*54*)] (Fig. 3). The two approaches have their own limitations: (i) for the ^{60}Fe-^{60}Ni system, uncertainties exist on the bulk silicate Fe/Ni and assumptions must be made on the $\varepsilon^{60}Ni$ homogeneity and secondary perturbations of the isochrons, and (ii) for the ^{182}Hf-^{182}W system, the Hf/W ratio can be fractionated at different levels in the various members of the angrites and HED meteorites after core segregation during mantle and crust differentiation processes (*54*). The

two systems share the limitation that metal segregation can be a multistage process. Despite these limitations, the two systems point to a very early differentiation (Fig. 3), implying even more rapid and early accretion.

Evolution of the EC 002 parent body

Dating metal segregation in the source of EC 002 at $0.82^{+0.61}_{-0.60}$ Myr after CAIs has important implications. Because this is ~800 thousand years (kyr) earlier than the crystallization of the EC 002 parental melt (using the Pb-Pb absolute age of EC 002), it allows reconstructing part of the history of the body. Thermal modeling shows that an early quasi-instantaneous accretion of a body implies its global melting (*55*, *56*), preventing the preservation of a chondritic crust. However, the distribution pattern of rare earth elements in EC 002 shows it derived from around 25% partial melting of a noncarbonaceous chondritic reservoir, likely of LL chondrite composition (*23*). Furthermore, thermal modeling of the evolution of a parent body, growing by accretion of cold materials and undergoing simultaneously melting and differentiation due to the heat released by the decay of ^{26}Al, shows that partial melting [at around 1220°C, as indicated by EC 002 composition (*23*)] could have taken place in the chondritic crust stabilized on top of a magma ocean (*57*). On the other hand, the low abundance of highly siderophile elements (HSE) in EC 002 (*24*) indicates that its source underwent metal segregation at some stage, in agreement with the high Fe/Ni ratio modeled for the bulk silicate parent body (*52*). However, the requirement of a chondritic composition of lithophile elements in the source of EC 002 implies that it did not experience melting of silicates but only extraction of a metallic liquid. This is possible if the melting temperature of this liquid was substantially lower than 1220°C. As discussed in (*58*), the temperature of melting of the Fe-S liquid depends on the S and Fe content of the liquid, and at 1 atm, for an Fe-FeS system with Fe content less than 74 wt%, the melting temperature is below 1200°C. The Fe metal and FeS contents of LL3 chondrites range from 0.34 to 6.62 wt % and from 4.99 to 8.39 wt %, respectively (*59*), resulting in several LL3 chondrites having an Fe content in Fe metal + FeS phases <74 wt %. In addition, studies of the distribution of HSE in ordinary chondrites have shown that the Fe metal is the dominant host of HSE (*60*). Thus, upon heating at temperatures between 1000° and 1200°C, a rock with an LL3 chondrite composition could undergo melting of its metal Fe and troilite only, with melting beginning at the contact between these two phases. The resulting Fe-Ni-FeS liquid would incorporate most of the HSE of the rock and segregate when a melt fraction of 5%, i.e., the threshold for percolation (*61*), is reached. This would leave a solid silicate residue with chondritic lithophile components, while the Fe/Ni ratio can be fractionated to the value modeled for the EC 002 source (*52*).

Taking LL3 chondrites as the building block for the EC 002 parent body (EC 002 PB) and an Fe content of 10% [mass fraction; (*59*)], the thermal evolution of the PB has been modeled in case of a protracted accretion (*57*) (fig. S10). When considering that, for instance, the EC 002 PB reached a final radius of ~90 km after ~3 Myr of accretion of cold dust and pebbles on a nucleus of ~70 km formed nearly instantaneously at time zero, thermal modeling shows that (i) a chondritic crust forms and is preserved on top of a magma ocean, and (ii) this crust undergoes first a metal segregation event at around 1000°C before undergoing 25% partial melting of the silicates several hundred kyr later (fig. S10B). The metal segregation time can be constrained from the 1000°C isotherm at the radius where a 25% melt temperature is reached at 1.6 Myr (in fact a quasi-plateau). This gives 1.3 Myr after CAIs (fig. S10B) and is consistent within the errors with the estimation of $0.82^{+0.61}_{-0.60}$ Myr after CAIs based on the ^{60}Fe-^{60}Ni systematic of EC 002. This indicates that the scenario of differentiation of the EC 002 PB deduced from the ^{60}Fe-^{60}Ni data is physically and thermally feasible. It should be noted that this scenario also indicates that the most massive metal/silicate segregation is not related to the extraction of metal from the stabilized chondritic crust but to the formation of the magma ocean (from 0.49 to 3.44 Myr, fig. S10A), which resulted in an apparent core age of 0.55 Myr.

The accretion and differentiation history of the EC 002 parent body is quite different from other early formed (~4.56 billion years ago) andesitic meteorites such as GRA 06128/9 (*62*, *63*), NWA 11119 (*64*), and ALM-A (*65*), suggesting diverse styles of ESS volcanisms on planetesimals. Besides, plate tectonics, supposed to be the mechanism for forming the felsic crust of Earth [e.g., (*66*)], is not necessary for producing andesitic crusts on planetesimals.

MATERIALS AND METHODS

Sample preparation and chemical purification

The bulk fraction (E-1) of EC 002 was obtained from a large fragment (~2 g) and mineral fractions (E-2 to E-8) were separated from ~8 g rock slice of EC 002. Mineral separates were prepared using a hand magnet (E-5, magnetic part), sieving (E-4, <250 μm and E-6 < 80 μm), Frantz isodynamic magnetic separator (E-2 and E-3 with a current >1 A and a size <250 μm), and heavy liquid methylene iodide (D = 3.3 g/cm^3, E-7 with low density and E-8 with high density). Fractions E-1 to E-6 were washed with MQ water in an ultrasonic bath for 20 min while fractions E-7 and E-8 were precleaned with acetone twice in ultrasonic bath to remove any potential contamination from heavy liquid before rinsing with MQ water. Fraction E-2 was leached with hot 6N HCl (120°C) for 30 min on hotplates. Fractions E-2R and E-2L represent the residue and the leachate.

All fractions except the metal part (E-5) and the leachate (E-2L) were dissolved in sealed Savillex beakers using a mixture of ultrapure concentrated HF and HNO_3 (3:1) and heated at 120° to 140°C for 7 days. After drying down at 120°C, the samples were redissolved in 6 M HCl for three or four times to completely remove fluorides. Fraction E-5 was initially dissolved in 6 M HCl and then in a mixture of concentrated HF and HNO_3 (3:1). Other fractions (WR1, WR2, Px, Coarse mag, and Fines) came from the same aliquots used for Nd isotope analyses of a previous study (*20*). The Px and the Coarse mag fractions are the residues after 20 min leaching with 1 M HCl at room temperature (*20*).

To ensure complete removal of matrix elements, a meticulous five-step protocol (fig. S11, table S3) was used to purify Ni from EC 002 fractions as well as geo-standards AGV-2 and BHVO-2. The samples were loaded on a long column with 8.5 ml of cation resin AG50W-X12, which effectively eluted most of the major elements (e.g., Na, Al, Ca, Ti, Cr, and Fe) and trace elements (Li, B, V, REE, Pb, Th, and U) using 2 M HNO_3 + 0.5 M HF, while transitional elements (Co, Ni, Cu, and Zn) and Mg as well as part of Mn and K were collected later with the same acid (fig. S12). To minimize the blank contamination, less than 0.6 ml of Ni-spec resin (the main source of blank during the whole procedure) was used to remove Mg from Ni cut, following the procedure described in (*67*). The remaining Mn

and Mg was separated using ultrapure oxalic acid as described in (*68*). Step 1 of the protocol was repeated to further purify impurities introduced by organic reagents (the Ni collection was performed later in the procedure to account for the much lower load mass), and any residual Co, Cu, and Zn were effectively removed using 0.1 ml of anion resin AG1-X8 and 8 M HCl at the end of the process. Because the matrix of the mineral fractions of EC 002 is very different from geo-standards, examinations were conducted for each step to avoid any influence of the sample specificity (Supplementary Materials). Pure standard solution SRM 986 underwent a final step column to eliminate any Fe and Zn. Samples and standards were treated with concentrated HNO_3 before measurements to attack any organic material present. The total blank is negligible (~4 ng) and the yield is high enough (95%) for accurate mass-independent Ni isotope measurement.

Mass spectrometry analysis

Nickel isotopic compositions were analyzed using a Neptune plus MC-ICP-MS equipped with an Apex HF introduction system at Institut de Physique du Globe de Paris (IPGP). Faraday cups L3, L2, C, H1, and H2 were used to measure ^{57}Fe, ^{58}Ni, ^{60}Ni, ^{61}Ni, and ^{62}Ni isotopes, respectively. A medium resolution slit ($M/\Delta m \cong 5000$) was used to resolve polyatomic interferences, such as $^{40}Ar^{18}O^+$ on $^{58}Ni^+$. The measurement was conducted on the left shoulder of the peak plateau to avoid Ar oxide interference (e.g., the optimal measurement position is 59.880 for the last analytical session, fig. S13). The magnet drift was checked, and the measurement position was adjusted to be optimal before each analytical session. Jet sample cones were used in conjunction with X skimmer cones to improve the sensitivity and a gas mixture of Ar + N_2 was used for sample introduction to suppress oxide formation and increase stability of the signal. Nickel solutions [50 parts per billion (ppb)] were measured in 0.5 M HNO_3. At an uptake rate of 100 μl/min, the sensitivity for ^{58}Ni is ~160 V/ppm, which is at least twice higher than in previous studies (*10*, *69*). One analysis consisted of 25 cycles and the integration time for each cycle lasted 4.2 s to minimize the consumption of the samples. Despite the short acquisition time, the internal standard error of ^{60}Ni/^{58}Ni ratios during each analysis was remarkably low, at the magnitude of 10^{-6}. This high precision could be attributed to the excellent stability of the mass spectrometry and purity of the samples. The sample-standard bracketing method was used during the measurement and standard solution SRM 986 was measured before and after each analysis of sample solution. The signal of $^{58}Ni^+$ of the acid used for diluting standards and samples was monitored before each session and was smaller than 0.008 V, which is negligible compared to that in the 50 ppb sample solutions (~8 V). The signal of $^{57}Fe^+$ was used to monitor the interference of $^{58}Fe^+$ on $^{58}Ni^+$, which shows that all the samples after chemistry purification have an Fe/Ni ratio lower than 10^{-4}; thus, no corresponding corrections have been performed. A small aliquot of original sample solutions was kept for the measurement of Fe/Ni ratios using an Agilent 7900 Q-ICP-MS in IPGP.

Supplementary Materials

The PDF file includes:

Supplementary Text
Figs. S1 to S13
Legend for table S1
Tables S2 and S3
References

Other Supplementary Material for this manuscript includes the following:

Table S1

REFERENCES AND NOTES

1. A. M. Davis, Short-lived nuclides in the early solar system: Abundances, origins, and applications. *Annu. Rev. Nucl. Part. Sci.* **72**, 339–363 (2022).
2. T. L. Norris, A. J. Gancarz, D. J. Rokop, K. W. Thomas, Half-life of ^{26}Al. *J. Geophys. Res.* **88**, B331–B333 (1983).
3. T. Lee, D. A. Papanastassiou, G. J. Wasserburg, Demonstration of ^{26}Mg excess in Allende and evidence for ^{26}Al. *Geophys. Res. Lett.* **3**, 41–44 (1976).
4. H. C. Urey, The cosmic abundances of potassium, uranium, and thorium and the heat balances of the Earth, the Moon, and Mars. *Proc. Natl. Acad. Sci. U.S.A.* **41**, 127–144 (1955).
5. G. Rugel, T. Faestermann, K. Knie, G. Korschinek, M. Poutivtsev, D. Schumann, N. Kivel, I. Günther-Leopold, R. Weinreich, M. Wohlmuther, New measurement of the Fe 60 half-life. *Phys. Rev. Lett.* **103**, 072502 (2009).
6. A. Shukolyukov, G. W. Lugmair, Live iron-60 in the early solar system. *Science* **259**, 1138–1142 (1993).
7. W. Neumann, D. Breuer, T. Spohn, Differentiation and core formation in accreting planetesimals. *Astron. Astrophys.* **543**, 141 (2012).
8. G. Quitte, A. N. Halliday, B. S. Meyer, A. Markowski, C. Latkoczy, D. Guenther, Correlated iron 60, nickel 62, and zirconium 96 in refractory inclusions and the origin of the solar system. *Astrophys. J.* **655**, 678–684 (2007).
9. F. Moynier, J. Blichert-Toft, K. Wang, G. F. Herzog, F. Albarede, The elusive ^{60}Fe in the solar nebula. *Astrophys. J.* **741**, 71 (2011).
10. H. L. Tang, N. Dauphas, Abundance, distribution, and origin of Fe-60 in the solar protoplanetary disk. *Earth Planet. Sci. Lett.* **359**, 248–263 (2012).
11. D. L. Cook, B. S. Meyer, M. Schönbächler, Iron and nickel isotopes in IID and IVB iron meteorites: Evidence for admixture of an SN II component and implications for the initial abundance of ^{60}Fe. *Astrophys. J.* **917**, 59 (2021).
12. R. K. Mishra, J. N. Goswami, Fe–Ni and Al–Mg isotope records in UOC chondrules: Plausible stellar source of ^{60}Fe and other short-lived nuclides in the early Solar System. *Geochim. Cosmochim. Acta* **132**, 440–457 (2014).
13. S. Mostefaoui, G. W. Lugmair, P. Hoppe, ^{60}Fe: A heat source for planetary differentiation from a nearby supernova explosion. *Astrophys. J* **625**, 271–277 (2005).
14. R. K. Mishra, M. Chaussidon, Fossil records of high level of ^{60}Fe in chondrules from unequilibrated chondrites. *Earth Planet. Sci. Lett.* **398**, 90–100 (2014).
15. M. Telus, G. R. Huss, R. C. Ogliore, K. Nagashima, S. Tachibana, Recalculation of data for short-lived radionuclide systems using less-biased ratio estimation. *Meteorit. Planet. Sci.* **47**, 2013–2030 (2012).
16. M. Telus, G. R. Huss, R. C. Ogliore, K. Nagashima, D. L. Howard, M. G. Newville, A. G. Tomkins, Mobility of iron and nickel at low temperatures: Implications for ^{60}Fe–^{60}Ni systematics of chondrules from unequilibrated ordinary chondrites. *Geochim. Cosmochim. Acta* **178**, 87–105 (2016).
17. R. Trappitsch, P. Boehnke, T. Stephan, M. Telus, M. R. Savina, O. Pardo, A. M. Davis, N. Dauphas, M. J. Pellin, G. R. Huss, New constraints on the abundance of ^{60}Fe in the early solar system. *Astrophys. J.* **857**, L15 (2018).
18. J. Kodolányi, P. Hoppe, C. Vollmer, J. Berndt, M. Müller, Iron-60 in the early solar system revisited: Insights from in situ isotope analysis of chondritic troilite. *Astrophys. J.* **929**, 107 (2022).
19. H. Tang, N. Dauphas, Low ^{60}Fe abundance in Semarkona and Sahara 99555. *Astrophys. J.* **802**, 22 (2015).
20. L. Fang, P. Frossard, M. Boyet, A. Bouvier, J.-A. Barrat, M. Chaussidon, F. Moynier, Half-life and initial Solar System abundance of ^{146}Sm determined from the oldest andesitic meteorite. *Proc. Natl. Acad. Sci. U.S.A.* **119**, e2120933119 (2022).
21. J. A. Van Orman, D. J. Cherniak, N. T. Kita, Magnesium diffusion in plagioclase: Dependence on composition, and implications for thermal resetting of the ^{26}Al–^{26}Mg early solar system chronometer. *Earth Planet. Sci. Lett.* **385**, 79–88 (2014).
22. G. Quitté, M. Meier, C. Latkoczy, A. N. Halliday, D. Günther, Nickel isotopes in iron meteorites–nucleosynthetic anomalies in sulphides with no effects in metals and no trace of ^{60}Fe. *Earth Planet. Sci. Lett.* **242**, 16–25 (2006).
23. J.-A. Barrat, M. Chaussidon, A. Yamaguchi, P. Beck, J. Villeneuve, D. J. Byrne, M. W. Broadley, B. Marty, A 4,565-My-old andesite from an extinct chondritic protoplanet. *Proc. Natl. Acad. Sci. U.S.A.* **118**, e2026129118 (2021).
24. R. W. Nicklas, J. M. D. Day, K. G. Gardner-Vandy, A. Udry, Early silicic magmatism on a differentiated asteroid. *Nat. Geosci.* **15**, 696–699 (2022).
25. A. Anand, P. M. Kruttasch, K. Mezger, ^{53}Mn-^{53}Cr chronology and ε^{54}Cr-Δ^{17}O genealogy of Erg Chech 002: The oldest andesite in the solar system. *Meteorit. Planet. Sci.* **57**, 2003–2016 (2022).
26. K. Zhu, H. Becker, S.-J. Li, Y. Fan, X.-N. Liu, T. Elliott, Radiogenic chromium isotope evidence for the earliest planetary volcanism and crust formation in the Solar system. *Mon. Not. R. Astron. Soc. Lett.* **515**, L39–L44 (2022).

27. G. Quitté, A. Markowski, C. Latkoczy, A. Gabriel, A. Pack, Iron-60 heterogeneity and incomplete isotope mixing in the early solar system. *Astrophys. J.* **720**, 1215–1224 (2010).
28. J. W. Gramlich, L. A. Machlan, I. L. Barnes, P. J. Paulsen, Absolute isotopic abundance ratios and atomic weight of a reference sample of nickel. *J. Res. Natl. Inst. Stan.* **94**, 347–356 (1989).
29. W. A. Russell, D. A. Papanastassiou, T. A. Tombrello, Ca isotope fractionation on the Earth and other solar system materials. *Geochim. Cosmochim. Acta* **42**, 1075–1090 (1978).
30. K. I. Mahon, The New "York" regression: Application of an improved statistical method to geochemistry. *Int. Geol. Rev.* **38**, 293–303 (1996).
31. T. Stephan, R. Trappitsch, Reliable uncertainties: Error correlation, rotated error bars, and linear regressions in three-isotope plots and beyond. *Int. J. Mass Spectrom.* **491**, 117053 (2023).
32. P. M. Reger, Y. Roebbert, W. Neumann, A. Gannoun, M. Regelous, W. H. Schwarz, T. Ludwig, M. Trieloff, S. Weyer, A. Bouvier, Al-Mg and U-Pb chronological records of Erg Chech 002 ungrouped achondrite meteorite. *Geochim. Cosmochim. Acta* **343**, 33–48 (2023).
33. J. N. Connelly, J. Bollard, E. Amsellem, M. Schiller, K. K. Larsen, M. Bizzarro, Evidence for very early planetesimal formation and ^{26}Al/^{27}Al heterogeneity in the protoplanetary disk. *Astrophys. J. Lett.* **952**, L33 (2023).
34. E. Krestianinov, Y. Amelin, Q.-Z. Yin, P. Cary, M. H. Huyskens, A. Miller, S. Dey, Y. Hibiya, H. Tang, E. D. Young, A. Pack, T. Di Rocco, Igneous meteorites suggest Aluminium-26 heterogeneity in the early Solar Nebula. *Nat. Commun.* **14**, 4940 (2023).
35. J. N. Connelly, M. Bizzarro, A. N. Krot, Å. Nordlund, D. Wielandt, M. A. Ivanova, The absolute chronology and thermal processing of solids in the solar protoplanetary disk. *Science* **338**, 651–655 (2012).
36. M. Piralla, J. Villeneuve, N. Schnuriger, D. V. Bekaert, Y. Marrocchi, A unified chronology of dust formation in the early solar system. *Icarus* **394**, 115427 (2023).
37. S. J. Desch, D. R. Dunlap, C. D. Williams, P. Mane, E. T. Dunham, Statistical chronometry of meteorites: II. Initial abundances and homogeneity of short-lived radionuclides. *Icarus* **402**, 115611 (2023).
38. G. A. Brennecka, M. Wadhwa, Uranium isotope compositions of the basaltic angrite meteorites and the chronological implications for the early Solar System. *Proc. Natl. Acad. Sci. U.S.A.* **109**, 9299–9303 (2012).
39. D. P. Glavin, A. Kubny, E. Jagoutz, G. W. Lugmair, Mn-Cr isotope systematics of the D'Orbigny angrite. *Meteorit. Planet. Sci.* **39**, 693–700 (2004).
40. A. Trinquier, J. L. Birck, C. J. Allègre, C. Göpel, D. Ulfbeck, ^{53}Mn–^{53}Cr systematics of the early Solar System revisited. *Geochim. Cosmochim. Acta* **72**, 5146–5163 (2008).
41. R. K. Mishra, K. K. Marhas, Abundance of ^{60}Fe inferred from nanoSIMS study of QUE 97008 (L3. 05) chondrules. *Earth Planet. Sci. Lett.* **436**, 71–81 (2016).
42. M. Telus, G. R. Huss, K. Nagashima, R. C. Ogliore, S. Tachibana, In situ ^{60}Fe-^{60}Ni systematics of chondrules from unequilibrated ordinary chondrites. *Geochim. Cosmochim. Acta* **228**, 342–457 (2018).
43. J. Render, G. A. Brennecka, S.-J. Wang, L. E. Wasylenki, T. Kleine, A distinct nucleosynthetic heritage for early solar system solids recorded by Ni isotope signatures. *Astrophys. J.* **862**, 26 (2018).
44. G. Quitté, C. Latkoczy, M. Schönbächler, A. N. Halliday, D. Günther, ^{60}Fe–^{60}Ni systematics in the eucrite parent body: A case study of Bouvante and Juvinas. *Geochim. Cosmochim. Acta* **75**, 7698–7706 (2011).
45. R. Steele, C. Coath, M. Regelous, T. Elliott, S. Russell, Neutron-poor nickel isotope anomalies in meteorites. *Astrophys. J.* **758**, 59 (2012).
46. J. A. M. Nanne, F. Nimmo, J. N. Cuzzi, T. Kleine, Origin of the non-carbonaceous–carbonaceous meteorite dichotomy. *Earth Planet. Sci. Lett.* **511**, 44–54 (2019).
47. G. J. Wasserburg, R. Gallino, M. Busso, A test of the supernova trigger hypothesis with ^{60}Fe and ^{26}Al. *Astrophys. J.* **500**, L189–L193 (1998).
48. S. W. Jones, H. Möller, C. L. Fryer, C. J. Fontes, R. Trappitsch, W. P. Even, A. Couture, M. R. Mumpower, S. Safi-Harb, ^{60}Fe in core-collapse supernovae and prospects for X-ray and gamma-ray detection in supernova remnants. *Mon. Not. R. Astron. Soc.* **485**, 4287–4310 (2019).
49. M. Pignatari, E. Zinner, P. Hoppe, C. J. Jordan, B. K. Gibson, R. Trappitsch, F. Herwig, C. Fryer, R. Hirschi, F. X. Timmes, Carbon-rich presolar grains from massive stars: Subsolar ^{12}C/^{13}C and ^{14}N/^{15}N ratios and the mystery of ^{15}N. *Astrophys. J. Lett.* **808**, L43 (2015).
50. G. R. Huss, B. S. Meyer, G. Srinivasan, J. N. Goswami, S. Sahijpal, Stellar sources of the short-lived radionuclides in the early solar system. *Geochim. Cosmochim. Acta* **73**, 4922–4945 (2009).
51. K. Lodders, Solar system abundances and condensation temperatures of the elements. *Astrophys. J.* **591**, 1220–1247 (2003).
52. C. Cartier, L. Llado, H. Pirotte, L. Tissandier, O. Namur, M. Collinet, S.-J. Wang, B. Charlier, Partitioning of nickel and cobalt between metal and silicate melts: Expanding the oxy-barometer to reducing conditions. *Geochim. Cosmochim. Acta* **367**, 142–164 (2024).
53. T. Kleine, K. Mezger, C. Münker, H. Palme, A. Bischoff, ^{182}Hf-^{182}W isotope systematics of chondrites, eucrites, and martian meteorites: Chronology of core formation and early mantle differentiation in Vesta and Mars. *Geochim. Cosmochim. Acta* **68**, 2935–2946 (2004).
54. T. Kleine, U. Hans, A. J. Irving, B. Bourdon, Chronology of the angrite parent body and implications for core formation in protoplanets. *Geochim. Cosmochim. Acta* **84**, 186–203 (2012).
55. T. S. Kruijer, M. Touboul, M. Fischer-Gödde, K. R. Bermingham, R. J. Walker, T. Kleine, Protracted core formation and rapid accretion of protoplanets. *Science* **344**, 1150–1154 (2014).
56. E. Kaminski, A. Limare, B. Kenda, M. Chaussidon, Early accretion of planetesimals unraveled by the thermal evolution of the parent bodies of magmatic iron meteorites. *Earth Planet. Sci. Lett.* **548**, 116469 (2020).
57. C. Sturtz, A. Limare, M. Chaussidon, É. Kaminski, Structure of differentiated planetesimals: A chondritic fridge on top of a magma ocean. *Icarus* **385**, 115100 (2022).
58. R. Brett, P. M. Bell, Melting relations in the Fe-rich portion of the system Fe-FeS at 30 kb pressure. *Earth Planet. Sci. Lett.* **6**, 479–482 (1969).
59. E. Jarosewich, Chemical analyses of meteorites at the Smithsonian Institution: An update. *Meteorit. Planet. Sci.* **41**, 1381–1382 (2006).
60. Y. Kadlag, H. Becker, Origin of highly siderophile and chalcogen element fractionations in the components of unequilibrated H and LL chondrites. *Geochemistry* **77**, 105–119 (2017).
61. T. Yoshino, M. J. Walter, T. Katsura, Core formation in planetesimals triggered by permeable flow. *Nature* **422**, 154–157 (2003).
62. J. M. D. Day, R. D. Ash, Y. Liu, J. J. Bellucci, D. R. Iii, W. F. McDonough, R. J. Walker, L. A. Taylor, Early formation of evolved asteroidal crust. *Nature* **457**, 179–182 (2009).
63. C. K. Shearer, P. V. Burger, C. Neal, Z. Sharp, L. Spivak-Birndorf, L. Borg, V. A. Fernandes, J. J. Papike, J. Karner, M. Wadhwa, A. Gaffney, J. Shafer, J. Geissman, N. V. Atudorei, C. Herd, B. P. Weiss, P. L. King, S. A. Crowther, J. D. Gilmour, Non-basaltic asteroidal magmatism during the earliest stages of solar system evolution: A view from Antarctic achondrites Graves Nunatak 06128 and 06129. *Geochim. Cosmochim. Acta* **74**, 1172–1199 (2010).
64. P. Srinivasan, D. R. Dunlap, C. B. Agee, M. Wadhwa, D. Coleff, K. Ziegler, R. Zeigler, F. M. McCubbin, Silica-rich volcanism in the early solar system dated at 4.565 Ga. *Nat. Commun.* **9**, 3036 (2018).
65. A. Bischoff, M. Horstmann, J.-A. Barrat, M. Chaussidon, A. Pack, D. Herwartz, D. Ward, C. Vollmer, S. Decker, Trachyandesitic volcanism in the early Solar System. *Proc. Natl. Acad. Sci. U.S.A.* **111**, 12689–12692 (2014).
66. I. H. Campbell, S. R. Taylor, No water, no granites—No oceans, no continents. *Geophys. Res. Lett.* **10**, 1061–1064 (1983).
67. G. V. Makhatadze, M. Schiller, M. Bizzarro, High precision nickel isotope measurements of early Solar System materials and the origin of nucleosynthetic disk variability. *Geochim. Cosmochim. Acta* **343**, 17–32 (2023).
68. D. M. Ratnayake, R. Tanaka, E. Nakamura, Novel nickel isolation procedure for a wide range of sample matrices without using dimethylglyoxime for isotope measurements using MC-ICP-MS. *Anal. Chim. Acta* **1181**, 338934 (2021).
69. G. Quitté, F. Oberli, Quantitative extraction and high precision isotope measurements of nickel by MC-ICPMS. *J. Anal. At. Spectrom* **21**, 1249–1255 (2006).
70. J. Gattacceca, F. M. McCubbin, J. Grossman, A. Bouvier, E. Bullock, H. Chennaoui Aoudjehane, V. Debaille, M. D'orazio, M. Komatsu, B. Miao, The Meteoritical Bulletin, No. 109. *Meteorit. Planet. Sci.* **56**, 1626–1630 (2021).
71. M. Regelous, T. Elliott, C. D. Coath, Nickel isotope heterogeneity in the early Solar System. *Earth Planet. Sci. Lett.* **272**, 330–338 (2008).
72. R. C. J. Steele, T. Elliott, C. D. Coath, M. Regelous, Confirmation of mass-independent Ni isotopic variability in iron meteorites. *Geochim. Cosmochim. Acta* **75**, 7906–7925 (2011).
73. A. Halliday, M. Rehkämper, D.-C. Lee, W. Yi, Early evolution of the Earth and Moon: New constraints from Hf-W isotope geochemistry. *Earth Planet. Sci. Lett.* **142**, 75–89 (1996).
74. C. L. Harper Jr., S. B. Jacobsen, Evidence for ^{182}Hf in the early Solar System and constraints on the timescale of terrestrial accretion and core formation. *Geochim. Cosmochim. Acta* **60**, 1131–1153 (1996).
75. S. B. Jacobsen, The Hf-W isotopic system and the origin of the Earth and Moon. *Annu. Rev. Earth Planet. Sci.* **33**, 531–570 (2005).
76. K. V. Krishnamurty, G. M. Harris, The chemistry of the metal oxalato complexes. *Chem. Rev.* **61**, 213–246 (1961).
77. A. N. Krot, Y. Amelin, P. Cassen, A. Meibom, Young chondrules in CB chondrites from a giant impact in the early Solar System. *Nature* **436**, 989–992 (2005).
78. N. T. Kita, T. Ushikubo, Evolution of protoplanetary disk inferred from ^{26}Al chronology of individual chondrules. *Meteorit. Planet. Sci.* **47**, 1108–1119 (2012).
79. H. Tang, N. Dauphas, ^{60}Fe–^{60}Ni chronology of core formation in Mars. *Earth Planet. Sci. Lett.* **390**, 264–274 (2014).
80. K. Lodders, Relative atomic solar system abundances, mass fractions, and atomic masses of the elements and their isotopes, composition of the solar photosphere, and compositions of the major chondritic meteorite groups. *Space Sci. Rev.* **217**, 44 (2021).
81. W. Dai, F. Moynier, L. Fang, J. Siebert, K-Ca dating and Ca isotope composition of the oldest Solar System lava, Erg Chech 002. *Geochem. Perspect. Let.* **24**, 33–37 (2023).

Acknowledgments: We thank P. Burckel, D. Rigoussen, D. Ratnayake, and T.-H. Luu for help on chemistry work and R. Tartèse and J.-A. Barrat for discussions. **Funding:** This work was supported by ERC grant 101001282 (METAL) to F.M., Region Île-de-France SESAME grant nos. 12015908 and EX047016 to F.M., IdEx Université de Paris grant ANR-18-IDEX-0001 to F.M., DIM ACAV+ to F.M., and the China Scholarship Council for a PhD fellowship (#202004910297) to L.F.
Author contributions: Conceptualization: L.F., F.M., M.C., and A.L. Methodology: L.F., F.M., M.C., A.L., J.V., and G.V.M. Validation: L.F., F.M., and M.C. Formal analysis: L.F., M.C., and A.L. Data curation: L.F. Software: A.L. Resources: F.M. Investigation: L.F. and M.C. Visualization: L.F., M.C., and A.L. Funding acquisition: F.M. Project administration: F.M. and M.C. Supervision: F.M. Writing—original draft: L.F. and M.C. Writing—review and editing: L.F., F.M., M.C., A.L., J.V., and G.V.M. **Competing interests:** The authors declare that they have no competing interests. **Data and materials availability:** All data needed to evaluate the conclusions in the paper are present in the paper and/or the Supplementary Materials.

Submitted 18 April 2024
Accepted 4 December 2024
Published 8 January 2025
10.1126/sciadv.adp9381